High-Pressure Preparation, Crystal Structure, Magnetic Properties, and Phase Transitions in $GdNiO_3$ and $DyNiO_3$ Perovskites

J. A. Alonso,*,† M. J. Martínez-Lope,† M. T. Casais,† J. L. Martínez,† G. Demazeau,‡ A. Largeteau,‡ J. L. García-Muñoz,§ A. Muñoz,|| and M. T. Fernández-Díaz⊥

Instituto de Ciencia de Materiales de Madrid, C.S.I.C., Cantoblanco, E-28049 Madrid, Spain; Ecole Nationale Supérieure de Chimie et Physique de Bordeaux, BP 108, F-33402 Talence Cedex, France; Institut de Ciència de Materials de Barcelona, C.S.I.C., Campus UAB, Bellaterra, E−08193 Barcelona, Spain; Depto. de Física, EPS, University Carlos III, Butarque 15, Leganés, E-28911 Madrid, Spain; and Institut Laue-Langevin, B.P. 156, F-38042 Grenoble Cedex 9, France

Received March 15, 1999. Revised Manuscript Received June 1, 1999

Strongly distorted $RNiO_3$ (R = Gd, Dy) perovskites, containing Ni^{3+}, have been prepared under high-pressure conditions: 90 MPa of O_2 pressure (R = Gd) or 2 GPa of hydrostatic pressure in the presence of $KClO_4$ (R = Dy). These materials have been characterized by X-ray diffraction, neutron powder diffraction (NPD) (for $DyNiO_3$), DSC, magnetic measurements, and specific heat measurements. In contrast with the next member of the series, $HoNiO_3$, which shows a subtle monoclinic distortion at room temperature, $DyNiO_3$ exhibits orthorhombic symmetry, as shown by NPD data. A noticeable distortion is observed in NiO_6 octahedra, at variance with the almost regular octahedra exhibited by the first members (R = La, Pr, Nd) of the series: it is interpreted as a manifestation of the Jahn−Teller character of the Ni^{3+} cation, enhanced in the $RNiO_3$ perovskites with heavier rare earths, showing weaker, less covalent Ni−O bonds. DSC measurements show sharp endothermic peaks at 510.9 K (Gd) and 564.1 K (Dy) in the heating run, which have been assigned to the corresponding metal−insulator transitions of both charge-transfer perovskites, based on the analogous behavior observed for the precedent members of the $RNiO_3$ series. Subtle slope variations in the susceptibility vs *T* curves, highly dominated by the strong paramagnetic signal of Gd^{3+} and Dy^{3+}, indicate the onset of antiferromagnetic ordering of the Ni^{3+} sublattice, confirmed by specific heat measurements, below T_N values of 185 and 154 K, respectively. Additionally, the Dy^{3+} sublattice becomes ordered below 8 K.

Introduction

Within the broad family of transition metal oxide perovskites, the rare-earth nickelates $RNiO_3$ form a particularly interesting series. Synthesized for the first time by Demazeau et al.[1] in 1971 and completely forgotten for almost 20 years, these compounds have regained interest since the discovery of metal−insulator (MI) transitions in the Nd,[2,3] Pr, and Sm[2] compounds. In this family of perovskite oxides the MI transition had been described to occur without any noticeable changes in lattice symmetry, making easier the study of the different phenomena involved.[4] The transition temperature (T_{MI}) rises systematically as the rare-earth size becomes smaller, i.e., as the distortion of the perovskite with respect to the ideal structure (aristotype) increases.[5] It has been suggested that the MI transition is probably caused by the closing of the charge-transfer gap, induced by an increase in the electronic bandwidth.[5] For $LaNiO_3$ the large size of La determines a slightly distorted rhombohedral structure (space group $R\bar{3}c$) which, in fact, keeps its metallic character down to 1.5 K, showing no MI transition.[6] $RNiO_3$ oxides (R = Pr, Nd, Sm, Eu) are orthorhombic, crystallize in the $GdFeO_3$ structure (space group *Pbnm*), and exhibit MI transitions at 130 K (Pr), 200 K (Nd), 400 K (Sm), and 460 K (Eu).[5,7] For $PrNiO_3$ and $NdNiO_3$ the T_{MI} coincides with the paramagnetic−antiferromagnetic transition (T_N), but for R = Sm or smaller rare-earth cations, T_N is lower than T_{MI}, in such a way that there exists an intermediate field in which $RNiO_3$ are in an insulating and paramagnetic regime.

* To whom correspondence must be addressed.
† Instituto de Ciencia de Materiales de Madrid.
‡ Ecole Nationale Supérieure de Chimie et Physique de Bordeaux.
§ Institut de Ciència de Materials de Barcelona.
|| Universidad Carlos III.
⊥ Institut Laue-Langevin.

(1) Demazeau, G.; Marbeuf, A.; Pouchard, M.; Hagenmuller, P. *J. Solid State Chem.* **1971**, *3*, 582.
(2) Lacorre, P.; Torrance, J. B.; Pannetier, J.; Nazzal, A. I.; Wang P. W.; Huang, T.*C. J. Solid State Chem.* **1991**, *91*, 225.
(3) Vassiliou, J. K.; Hornbostel, M.; Ziebarth, R.; DiSalvo , F.J. *J. Solid State Chem.* **1989**, *81*, 208.
(4) Medarde, M. *J. Phys.: Condens. Matter* **1997**, *9*, 1679.
(5) Torrance, J. B.; Lacorre, P.; Nazzal, A. I.; Ansaldo, E. J.; Niedermayer, Ch. *Phys. Rev. B* **1992**, *45*, 8209.
(6) Goodenough, J. B.; Raccah, P. *J. Appl. Phys.* **1965**, *36*, 1031.
(7) Alonso, J. A.; Martínez-Lope M. J.; Rasines, I. *J. Solid State Chem.* **1995**, *120*, 170.

10.1021/cm991033k CCC: $18.00
Published on Web 08/07/1999

The existence of electronically induced subtle structural changes associated with the MI transition was reported.[8] The interest in rare-earth nickelates has been reinforced after the discovery of an unexpected magnetic ordering in $PrNiO_3$ and $NdNiO_3$ associated with the electronic localization.[9] In these compounds the magnetic ground state consists of alternating ferromagnetic and antiferromagnetic (AF) Ni−O−Ni couplings that violate the inversion center at the Ni site. More recently the observation of unusually large isotopic shifts of T_{MI} ($T_{MI}(^{18}O) - T_{MI}(^{16}O) \approx 10$ K)[10] confirms the importance of the electron−lattice coupling in these materials,[11] suggesting that the mechanism of the MI transition involves a strong electron−lattice interaction, the Jahn−Teller effect of the orbitally degenerated Ni^{3+} cations being the most likely origin for it.

The aforementioned physical properties have all been measured on polycrystalline materials prepared by annealing suitably reactive precursors in O_2 atmosphere, at pressures not higher than 20 MPa. Under these conditions, the perovskites for rare-earth cations as small as Eu^{3+} can be prepared. In fact, the totality of recent structural and physical−chemical studies on $RNiO_3$ perovskites deal with the members for R = La, Pr, Nd, Sm, and Eu. The difficulties found in the syntheses of $RNiO_3$ perovskites, inherent in the stabilization of Ni^{3+} cations, increase as the size of the rare-earth cation is reduced. For R^{3+} cations smaller than Eu^{3+}, the corresponding perovskites had not been prepared after the pioneering work of Demazeau et al.,[1] who synthesized the complete series of nickelates in 1971 in a belt-type equipment at 6 GPa using the "in situ" thermal decomposition of $KClO_3$ as the oxygen source.

In the course of our current research on rare-earth nickelates, we have been able to prepare $GdNiO_3$, at the very high O_2 pressure of 90 MPa, and $DyNiO_3$, $HoNiO_3$, and $YNiO_3$, in a piston-cylinder press at 2 GPa, in sealed gold capsules containing a mixture of the precursor oxides with $KClO_4$. These samples had not been prepared within the last 28 years, and nothing is known about their electronic and magnetic properties, metal−insulator transitions, or structural features. In this paper we address some of these open questions for $GdNiO_3$ and $DyNiO_3$, paying particular attention to the synthesis processes (Gd^{3+} is the smallest cation which can be stabilized under O_2 pressure; Dy^{3+} is the biggest, needing the stronger conditions provided by $KClO_4$ decomposition), the structural features, magnetic properties, and MI transitions.

Experimental Section

Together with Gd and Dy, the preparation of the rare-earth nickelate of Tb was at first tried by treatment under O_2 pressure of finely divided precursors obtained by soft chemistry procedures. Stoichiometric amounts of analytical grade R_2O_3 (R = Gd, Dy) or Tb_4O_7 and $Ni(NO_3)_2 \cdot 6H_2O$ were solved in citric acid, by adding several droplets of concentrated HNO_3. The citrate + nitrate solutions were slowly evaporated, leading to organic resins containing a random distribution of the involved cations at an atomic level. The green resins were first dried at 120 °C, leading to a very porous and voluminous "sponge-cake-like" material that was ground and slowly decomposed at temperatures up to 600 °C. All the organic materials and nitrates were eliminated in a subsequent treatment at 700 °C in air, for 12 h. This treatment gave rise to highly reactive precursor materials, amorphous to X-ray diffraction. Then, the precursors were put in gold sample holders and heated under high oxygen pressures of 9 MPa at 850 °C for 24 h each. Finally, the samples were left to slowly cool to room temperature in the reaction vessel.

This procedure led to perovskite $RNiO_3$ phases only for R = Gd. More strongly oxidizing conditions were then tried for R = Tb, Dy. For each compound, the precursor powder was mixed and thoroughly ground with $KClO_4$ (30% in weight), put into a gold capsule (8 mm diameter, 10 mm length), sealed, and placed in a cylindrical graphite heater. The reaction was carried out in a piston-cylinder press (Rockland Research Co.), at a pressure of 2 GPa at 900 °C for 20 min. Then, the material was quenched to room temperature and the pressure was subsequently released. The product was ground and washed in a dilute HNO_3 aqueous solution, to dissolve KCl coming from the decomposition of $KClO_4$ and to eliminate small amounts of unreacted NiO, R_2O_3, and $R_2O_2CO_3$ impurity phases; then, the powder samples were dried in air at 150 °C for 1 h.

The samples were characterized by X-ray powder diffraction (XRD) for phase identification and to assess phase purity. XRD patterns were collected with Cu Kα radiation in a Siemens D-501 goniometer controlled by a DACO-MP computer. The crystal structure of $DyNiO_3$ was studied by neutron powder diffraction (NPD) at room temperature: despite the absorbing nature of Dy and the relatively small amount of sample available, a good quality pattern could be collected at the D2B high-resolution diffractometer at ILL-Grenoble. A vanadium double-walled hollow cylindrical sample holder (8 mm diameter) was used to minimize absorption effects. The wavelength was 1.594 Å, and the counting time 8 h in the high-flux mode. The Rietveld program FULLPROF[12] was used to analyze the pattern. A pseudo-Voigt function was chosen to generate the line shape of the diffraction peaks. Since several peaks coming from the vanadium sample holder were detected in the pattern, the crystal structure of vanadium metal was introduced as a second phase in the final refinement. In the final run the following parameters were refined: background coefficients, zero-point, half-width, pseudo-Voigt, and asymmetry parameters for the peak shape; scale factors; positional, thermal isotropic, and unit-cell parameters. The much more severe absorbing character of Gd precluded the study of $GdNiO_3$ by neutron diffraction techniques.

Scanning electron microscopy (SEM) micrographs were taken with a Philips XL30 microscope at an accelerating voltage of 25 kV and magnification values up to 6500x. The $DyNiO_3$ SEM images were taken on as-grown, unpolished pellets.

Differential scanning calorimetry (DSC) experiments were performed in a Mettler TA3000 system equipped with a DSC30 unit, in the temperature range from 300 to 863 K. The heating rate was 10 °C min^{-1}, using about 70 mg of sample in each run.

Magnetic susceptibility was measured on powdered samples with a commercial SQUID magnetometer in the 1.5−300 K temperature range. Specific heat measurements were carried out on pelletized samples between 2 and 300 K by the relaxation pulse method, in a Physical Properties Measurement System from Quantum Design. The temperature stability was better than 0.2%; the accuracy better than 2% (compared to pure Cu). The lattice contribution to the specific heat was satisfactorily estimated by three Einstein oscillators at the frequencies of 200, 400, and 800 K.

(8) García-Muñoz, J. L.; Rodríguez-Carvajal, J.; Lacorre P.; Torrance, J. B. *Phys. Rev. B* **1992**, *46*, 4414.

(9) García-Muñoz, J. L.; Rodríguez-Carvajal J.; Lacorre, P. *Phys. Rev. B* **1994**, *50*, 978.

(10) Medarde, M.; Lacorre, P.; Conder, K.; Fauth F.; Furrer, A. *Phys. Rev. Lett.* 1998, *80*, 2397.

(11) Massa, N. E.; Alonso, J. A.; Martínez-Lope, M. J.*Phys. Rev. B* **1997**, *56*, 986.

(12) Rodríguez-Carvajal, J. *Physica (Amsterdam)* **1993**, *192B*, 55.

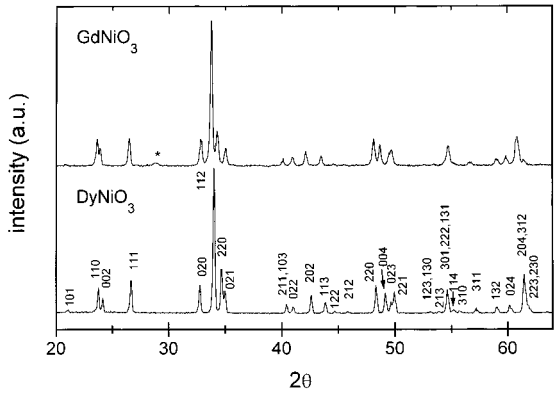

Figure 1. XRD patterns for $RNiO_3$, R = Gd, Dy. The star corresponds to Gd_2O_3. The $DyNiO_3$ pattern is indexed in an orthorhombic unit cell with $a \approx \sqrt{2}a_0$, $b \approx \sqrt{2}a_0$, $c \approx 2a_0$; $a_0 \approx$ 3.8 Å.

Results and Discussion

After the high oxygen pressure (90 MPa) treatment of the precursors, XRD patterns show that a $RNiO_3$ perovskite phase is only present for R = Gd (Figure 1a). The treatment in an hydrostatic piston-cylinder press at 2 GPa, together with $KClO_4$ as oxidizing agent, yields a perovskite phase for R = Dy (Figure 1b). In the case of R = Tb, mixtures of Tb_4O_7 and NiO were identified after both kinds of synthetic procedures. This is in agreement with the previous results of Demazeau et al., who were not able to prepare the hypothetical perovskite $TbNiO_3$ in their pioneering work,[1] even working at much superior pressures of 6 GPa. The trend of Tb to adopt the tetravalent oxidation state probably precludes the stabilization of Tb^{3+} in the perovskite structure, especially when the small size of Tb^{3+} makes necessary the use of strongly oxidizing conditions. This is in contrast with the easy preparation of $PrNiO_3$, despite the remarkable stability of Pr^{4+} cations, which in this case is overcome by the much higher stability of the perovskite structure containing Pr^{3+}, characterized by a larger tolerance factor.

$GdNiO_3$ perovskite seems to be the last member of the $RNiO_3$ series which can be prepared in a conventional high oxygen pressure furnace; the next stable perovskite member, $DyNiO_3$, already needs the much stronger oxidizing conditions provided by the in situ decomposition of $KClO_4$ in a sealed gold capsule. We have been able to prepare this phase by using an external pressure of 2 GPa, 3 times lower than that originally employed.[1] This allowed us to obtain, in compensation, a considerably larger amount of sample, of about 1 g after each run, making possible a more complete characterization of this material, including a neutron diffraction study. Probably, the decomposition of $KClO_4$, intimately mixed with the precursor powder, initially produces highly active atomic oxygen (O), which immediately reacts with the precursor at the working temperature (900 °C). The external pressure plays the role of containing the walls of the gold capsule against the residual internal pressure. It is difficult to make an estimation of the residual internal O_2 pressure after the reaction; from the stoichiometry of the mixture $KClO_4$/precursor, after total oxidation of Ni^{2+} to Ni^{3+}, and considering a density of the compressed powder of 95%, the residual O_2 pressure must be lower than 1.2 GPa.

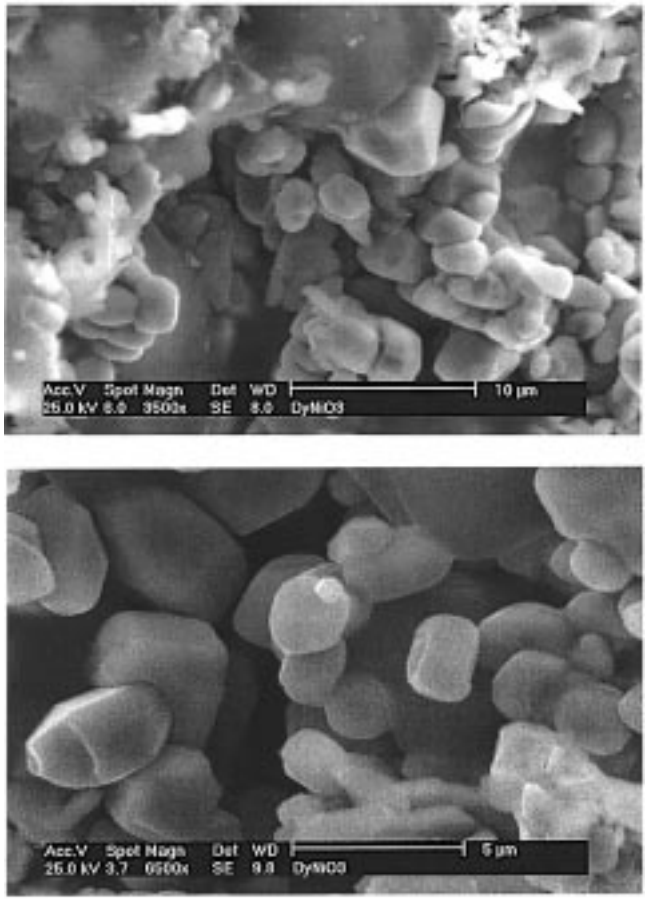

Figure 2. Scanning electron micrographs of as-grown $DyNiO_3$, taken at a magnification of (a) 3500×, and (b) 6500×.

Two electron micrographs (Figure 2) of as-grown $DyNiO_3$ taken at different magnifications illustrate the highly crystalline nature of this material. Figure 1a shows the presence of large cavities on the surface of the pellet (as-extracted from the gold capsule), probably due to the formation of O_2 bubbles coming from $KClO_4$ decomposition. The vitreous material observed on top of the picture is the resulting KCl product. $DyNiO_3$ microcrystals are distributed around the pores. Figure 2b shows the average shape and size of the $DyNiO_3$ microcrystals, in the range of 2−4 μm large.

Structural Features. The XRD patterns of $GdNiO_3$ and $DyNiO_3$ (once ground and washed to eliminate KCl) are characteristic of strongly distorted perovskites showing sharp, well-defined superstructure reflections (Figure 1). The structural refinement for $DyNiO_3$ was performed from room-temperature NPD data in the conventional *Pbnm* orthorhombic model, with unit-cell parameters related to a_0 (ideal cubic perovskite, $a_0 \approx$ 3.8 Å) as $a \approx \sqrt{2}a_0$, $b \approx \sqrt{2}a_0$, $c \approx 2a_0$, taking as starting atomic parameters those reported for the $EuNiO_3$ structure.[7] The final atomic coordinates, thermal factors, unit-cell parameters, and discrepancy factors after the refinements are included in Table 1. Figure 3 illustrates the goodness of the fit for the NPD profiles of $DyNiO_3$. A systematic study from synchrotron X-ray diffraction for $RNiO_3$ (R = Sm, Eu, Gd, Dy, Ho, and Y) allowed us to follow the structural and microstructural evolution along the series and will be published else-

Table 1. Unit-Cell and Atomic Parameters at Room Temperature for $RNiO_3$ (R = Gd, Dy), Refined from NPD Data (for R = Dy) and SXRD Data (R = Gd, from ref 13)[a]

	Gd	Dy
a (Å)	5.26063(5)	5.2063(1)
b (Å)	5.48544(5)	5.5056(1)
c (Å)	7.51116(7)	7.4455(1)
V (Å^3)	216.749(5)	213.418(6)
	R 4*c*(*x y* 1/4)	
x	0.9850(1)	0.9822(3)
y	0.06307(9)	0.0697(2)
B (Å^2)	0.44(1)	0.23(3)
	Ni 4*b*(1/2 0 0)	
B (Å^2)	0.33(5)	0.29(3)
	O1 4*c*(*x y* 1/4)	
x	0.0885(12)	0.0983(7)
y	0.4765(12)	0.4729(7)
B (Å^2)	0.25(18)	0.66(6)
	O2 8*d*(*x y z*)	
x	0.7038(9)	0.6964(5)
y	0.2974(9)	0.3010(5)
z	0.0471(7)	0.0489(3)
B (Å^2)	0.44(13)	0.67(4)
	Reliability factors	
χ^2	3.92	1.29
R_p (%)	9.0	2.09
R_{wp} (%)	11.2	2.58
R_{exp} (%)		2.27
R_I (%)	3.9	6.40

[a] Space group *Pbnm*, *Z* = 4.

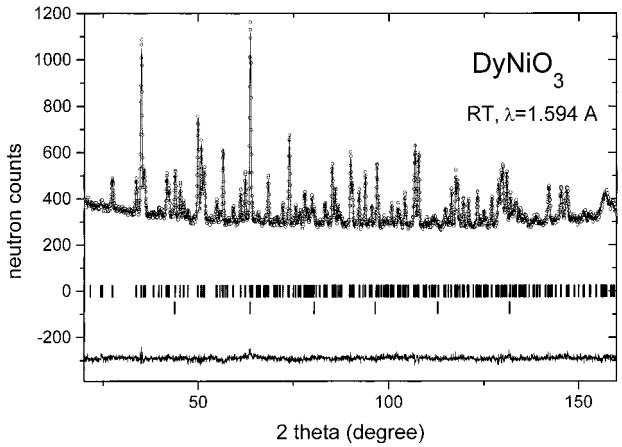

Figure 3. Observed (circles), calculated (full line), and difference (bottom) NPD Rietveld profiles for $DyNiO_3$ at room temperature. The two series of tick marks correspond to the allowed Bragg reflections for the main phase and vanadium coming from the double-walled sample holder.

where.[13] For the sake of comparison, the structural parameters of $GdNiO_3$ are also included in Table 1. The unit-cell parameters for $GdNiO_3$ and $DyNiO_3$ (Table 1) are very close to those reported by Demazeau et al.[1] It is worth mentioning that $c/\sqrt{2}$ lies between *a* and *b* parameters. This is the usual situation in perovskites where the primary distorting effect is steric. This is in contrast with $LaMnO_3$ perovskite in which the strong cooperative Jahn−Teller effect induces an orbital ordering, distorting the MnO_6 octahedra and giving rise to the so-called O′ structure, with $c/\sqrt{2} < a < b$.

Table 2 contains a selected list of distances and angles, and a view of the $DyNiO_3$ structure is shown in

(13) Alonso, J. A.; Martínez-Lope, M. J.; Casais, M. T.; Aranda, M. A. G.; Fernández-Díaz, M. T. *J. Am. Chem. Soc.* In press.

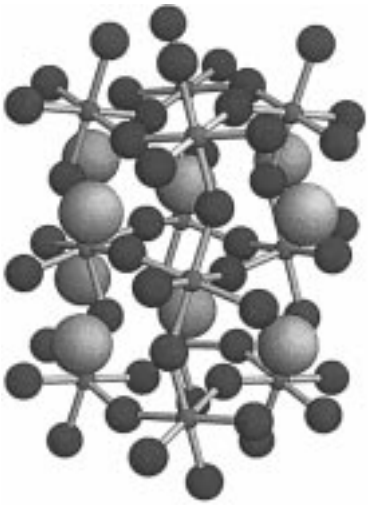

Figure 4. View of the structure of orthorhombic $DyNiO_3$. The *c* axis is vertical, and the *a* axis is from right to left. Large spheres represent Dy; corner-sharing NiO_6 octahedra are fairly tilted in the structure to optimize Dy−O bond lengths.

Table 2. Main Interatomic Distances (Å) and Angles (deg) for $RNiO_3$ (R = Gd, Dy) Perovskites

	Gd	Dy
	NiO_6 Octahedra	
Ni−O1 (×2)	1.939(2)	1.936(1)
Ni−O2 (×2)	1.984(5)	1.981(3)
Ni−O2 (×2)	1.946(5)	1.957(3)
⟨Ni−O⟩	1.956(4)	1.958(2)
Ni−O1−Ni (×2)	151.1(4)	148.03(4)
Ni−O2−Ni (×4)	150.4(3)	148.29(11)
⟨Ni−O−Ni⟩	150.6(3)	148.20(3)
	RO_8 Polyhedra	
R−O1	2.332(6)	2.301(4)
R−O1	3.055(7)	3.069(4)
R−O1	2.293(7)	2.248(4)
R−O2 (×2)	2.483(6)	2.465(3)
R−O2 (×2)	2.331(5)	2.301(2)
R−O2 (×2)	2.625(6)	2.589(2)
$\langle R-O\rangle_{8\ short}$	2.438(6)	2.407(3)

Figure 4. The orthorhombic perovskite structure of $RNiO_3$ (R = Gd, Dy) is fairly distorted due to the small size of the R^{3+} cations, which force the NiO_6 octahedra to tilt in order to optimize the R−O distances. It is worth mentioning that for the smallest Ho^{3+} and Y^{3+} cations a monoclinic distortion has been detected from SXRD data[13] in the insulating regime, below the MI transition. For instance, for $HoNiO_3$ at room temperature, a = 5.18200(4) Å, b = 5.51050(4) Å, c = 7.42336(5) Å, β = 90.084(1)°; space group $P2_1/n$. The possibility of existence of a very subtle monoclinic distortion in $DyNiO_3$, in the limit of the resolution of the SXRD data, could not be excluded in that former study.[13] Present neutron diffraction data for $DyNiO_3$ allow us to definitely rule out this possibility: a refinement in the $P2_1/n$ model diverges, leading to unreliable R factors, atomic parameters, and bond distances. The present study enables us to confirm that $DyNiO_3$ is not monoclinically distorted; it is the last member of the $RNiO_3$ series showing orthorhombic symmetry in the insulating regime.

A noticeable distortion is observed in the NiO_6 octahedra for $GdNiO_3$ and $DyNiO_3$: in the latter, Ni−O bond distances range between 1.936(1) and 1.981(2) Å. To quantify the relative distortion of the octahedra, we define the Δ_d parameter, concerning the deviation of

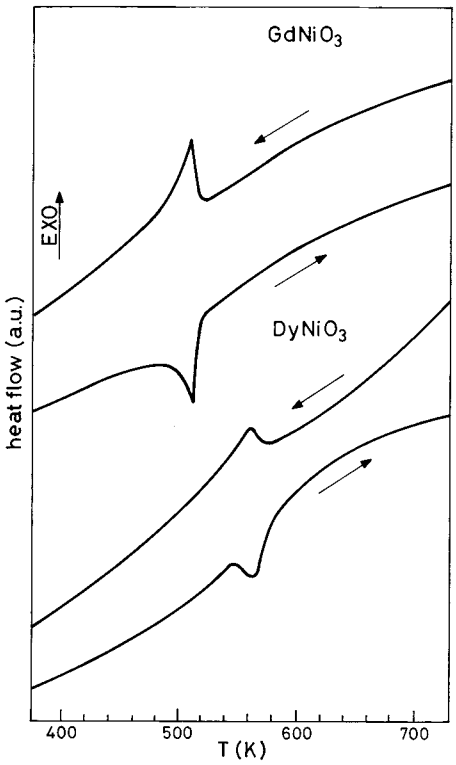

Figure 5. DSC curves for $RNiO_3$ (R = Gd, Dy) obtained on heating and cooling runs.

Ni−O distances with respect to the average ⟨Ni−O⟩ value, as $\Delta_d = (1/6)\sum_{n=1,6}[(d_n - \langle d\rangle)/\langle d\rangle]^2$. For R = Gd, Dy, Δ_d is 1.02×10^{-4} and 0.88×10^{-4}, respectively. For the sake of comparison, for Pr and Nd nickelates Δ_d values are as small as 10^{-7} and 3×10^{-6}, respectively, corresponding to almost regular octahedra. In $RNiO_3$, Ni^{3+} is a Jahn−Teller (JT) ion with a single electron in an orbitally degenerate ground state ($t^6_{2g}e^1_g$). The fact that no anisotropy could be detected in the NiO_6 octahedra for the largest rare-earth cations (R = La, Pr, Nd) was thought to be due to the strongly covalent character of the Ni−O bonds. The increased anisotropy of the NiO_6 octahedra, observed in a higher degree in $GdNiO_3$ and $DyNiO_3$, could be explained as a consequence of the manifestation of JT-induced distortions due to the progressive reduction of the covalent contribution of Ni−O bonds along the series. It is important to remember that for the lighter R members the existence of JT polarons has been recently demonstrated.[10,11] In $RNiO_3$ oxides, for sufficiently small R^{3+} cations, the electron−lattice interactions seem to be strong enough to drive a significant distortion of the NiO_6 octahedra, as shown in the most orthorhombically distorted members of the series, $GdNiO_3$ and $DyNiO_3$.

Metal−Insulator Transitions. Figure 5 shows the DSC curves for $RNiO_3$, R = Gd and Dy, obtained during the heating and cooling runs. The heating process exhibits a sharp endothermic peak centered at 510.9 and 564.1 K for Gd and Dy compounds, respectively; the reverse transition, showing an exothermic peak, is observed during the cooling run. By analogy with the DSC peaks observed at the metal-to-insulator transitions in the precedent members of the $RNiO_3$ series, we assign the peaks shown in Figure 5 for R = Gd and Dy to the corresponding first-order insulator-to-metal transitions of these perovskites. This assignment is tentative

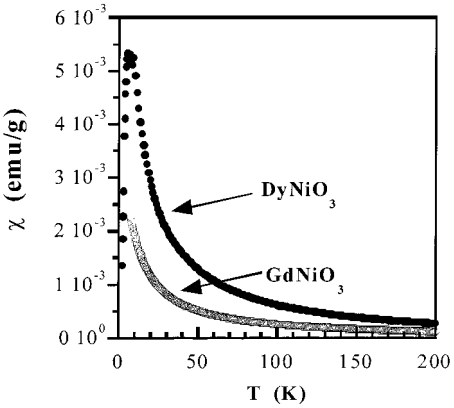

Figure 6. Temperature dependence of the dc magnetic susceptibility of $GdNiO_3$ and $DyNiO_3$.

(although very probable) and should be verified by resistivity measurements, not available at the present state of investigations due to the difficulties found in sintering pure $GdNiO_3$ and $DyNiO_3$. The observed thermal hysteresis observed by DSC is inherent in the first-order character of the MI transitions. The heat transfer accounts for the gain in energy corresponding to the electronic delocalization when reaching the metallic state, above this temperature.

Magnetic and Thermal Properties. Figure 6 shows the magnetic susceptibility vs temperature curve of $GdNiO_3$, recorded after a field-cooled process and measured in a magnetic field of 1 T. As expected, the temperature evolution of χ is largely dominated by the high Gd^{3+} moment ($\mu_{Gd} \approx 8\mu_B$, $8S_{7/2}$). Despite the difference between gadolinium and nickel moments, an anomaly could be detected between 185 and 200 K that tracks the magnetic ordering of Ni moments below that temperature. This is shown in Figure 7a, where we have represented the temperature evolution of $\chi T(T)$ in the interval 180−220 K. A change in the slope of χT is clearly observed within that temperature window. The specific heat measurement shown in Figure 8a also confirmed the presence of magnetic ordering below $T_N \approx 185$ K. The inset of Figure 8a shows the excess of specific heat after the subtraction of the lattice contribution. The entropy related to the AF ordering estimated from the excess of specific heat is 190 mJ mol^{-1} K^{-2}. There are no other magnetic transitions visible down to 7 K (the lowest temperature reached). The evolution of χT confirms that Gd moments remain disordered above 7 K. From the Curie−Weiss behavior fitted in the range 7−200 K, the effective paramagnetic moment is $\mu_{eff} = 7.66\ \mu_B$ (close to the expected value of 7.94 μ_B for the free Gd^{3+} ion) and $\theta_W = -1.9$ K. Unfortunately, it is not possible to investigate the magnetic ordering in this compound by neutron diffraction because of the high neutron absorption cross section of natural Gd.

The susceptibility of $DyNiO_3$ (measured in a magnetic field of 0.1 T) is shown in Figure 6. The Néel transition for Ni moments was found be $T_N \approx 154$ K from susceptibility and specific heat measurements (see, respectively, Figure 7b and Figure 8a). The specific heat, after subtraction of the lattice contribution, is shown in the upper inset of Figure 8a. The entropy associated with the long-range AF ordering is 754 mJ mol^{-1} K^{-2}, much higher than in the former case. In addition, and

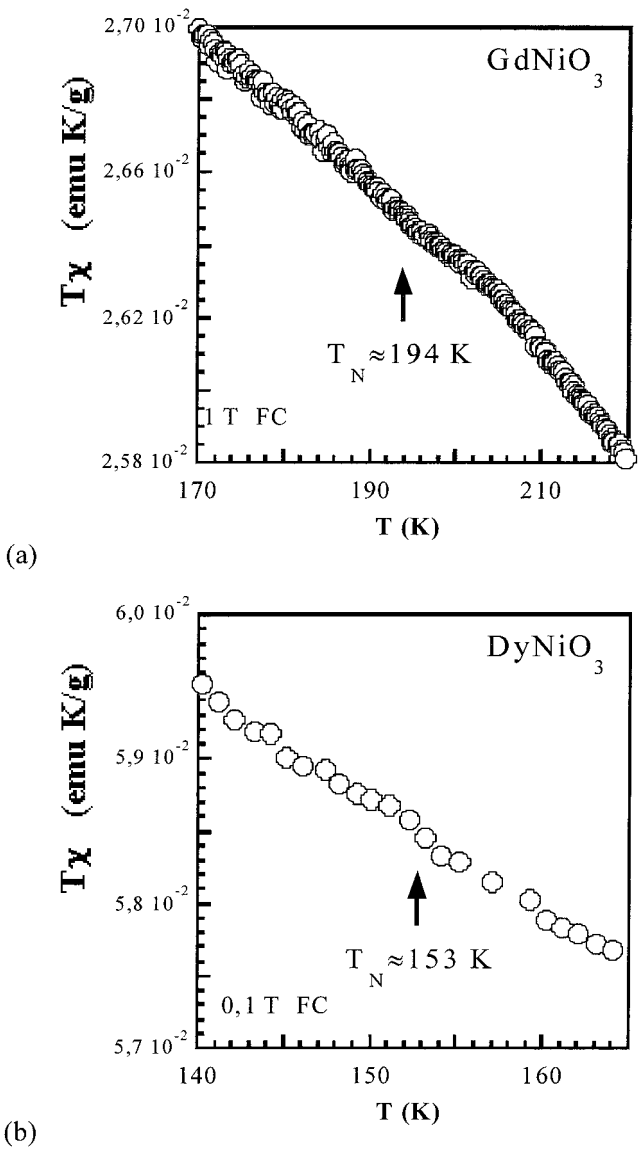

Figure 7. (a) χT plots for (a) $GdNiO_3$ (in the temperature interval of 180−220 K) and (b) $DyNiO_3$ (within the interval 140−165 K) showing the anomalies at the Néel temperatures.

conversely to the Gd perovskite, the susceptibility data detected a maximum in the low-temperature susceptibility, corresponding to the magnetic ordering of Dy^{3+} moments below $T_{Dy} \approx 8$ K. The low-temperature specific heat (Figure 8b) also shows the long-range AF ordering of the Dy sublattice at $T_N(Dy) = 8.5$ K (for $H = 0$). At lower temperature there is a second strong peak ($T_{max} = 3$K) related to a Schottky anomaly for a transition between two crystal-field levels of Dy^{3+}, with a Kramer doublet as the ground state. The application of an external magnetic field ($H = 1$T, 3T) breaks the degeneracy of the ground state, giving rise to the appearance of difference levels much closer in energy and suppressing the specific-heat peak to lower temperatures. The peak corresponding to $T_N(Dy)$ also shifts and spreads out under a magnetic field due to the reduction of entropy associated with the strong magnetization imposed by the external magnetic field. The effective moment obtained from the Curie−Weiss fit (Figure 9) in the intermediate region between 50 and 120 K (in which the Ni sublattice is already ordered, and the paramagnetic contribution comes only from Dy^{3+} cat-

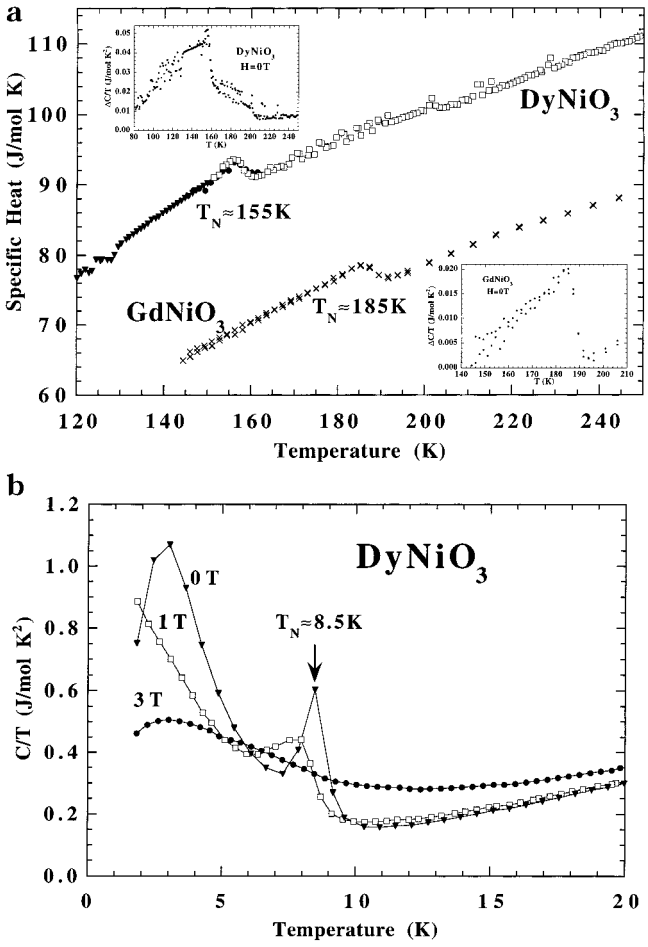

Figure 8. (a) Specific heat measurements indicating the magnetic ordering of the Ni sublattice for $GdNiO_3$ and $DyNiO_3$. The inset shows the excess specific heat associated with the AF ordering. (b) Low-temperature specific heat for $DyNiO_3$ at different applied magnetic fields.

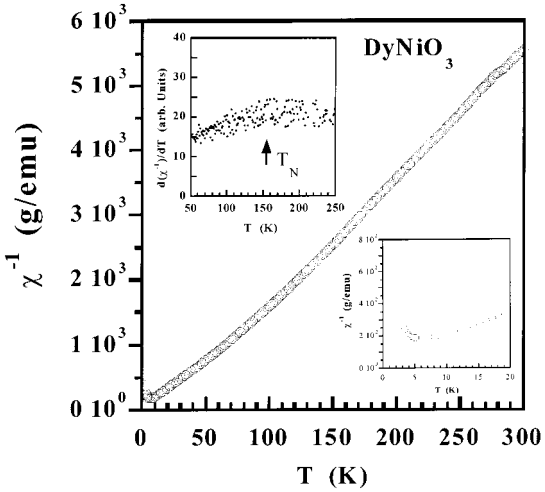

Figure 9. Inverse susceptibility of $DyNiO_3$. Insets: temperature derivative of the inverse susceptibility and the low-temperature region of $1/\chi(T)$.

ions) was 11.3 μ_B (only slightly bigger than 10.7 μ_B, the expected value for the free Dy^{3+} cation, $^6H_{15/2}$). The corresponding Weiss constant θ_W was 3.7 K, close to the temperature at which the susceptibility reaches a maximum. From the values of the Curie constant above T_N (154 K), we obtained a paramagnetic moment of $\mu_{eff} = 10.3\ \mu_B$ and $\theta_W = +23$ K.

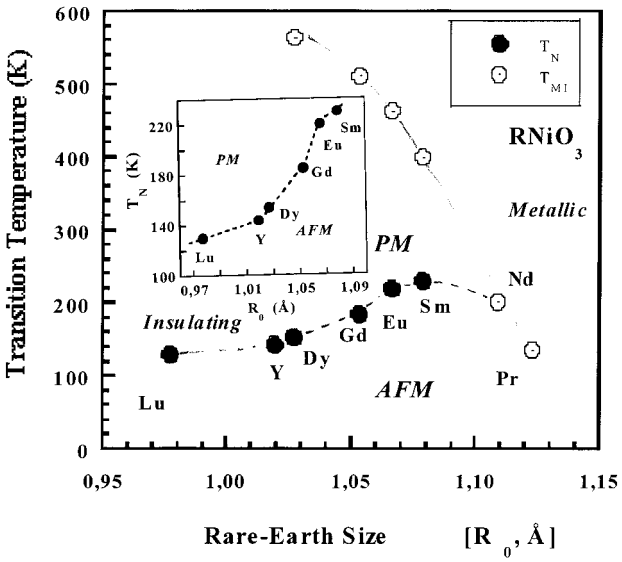

Figure 10. Evolution of the T_{MI} and T_N values upon varying the size of the rare earth along the $RNiO_3$ series. The metal−insulator transition temperatures are also shown for rare-earth cations larger than Gd^{3+}. Inset: detail of $T_N(R_0)$ for $RNiO_3$ samples with $T_N < T_{MI}$.

Phase Diagram. We recall that the Néel temperature was found to be 145 and 220 K for, respectively, $YNiO_3$[1] and $EuNiO_3$.[5] The phase diagram showing the evolution of T_N and T_{MI} values as a function of the structural distortion (governed by the R_0 size;[14] $R_0[Y^{3+}] = 1.019$ Å $< R_0[Dy^{3+}] = 1.027$ Å $< R_0[Gd^{3+}] = 1.053$ Å $< R_0[Eu^{3+}] = 1.066$ Å) has been represented in Figure 10. The MI temperature for $GdNiO_3$ and $DyNiO_3$ follows the monotonic variation observed for $RNiO_3$ with larger R^{3+} cations, although the expected variation rate decreases. It is interesting to note that the evolution of the Néel temperatures displays a nonmonotonic behavior as a function of the distortion. This has been illustrated in the inset of Figure 10. Note that there is a significant drop of the Néel temperature commensurate with the structural distortion between Eu and Dy. Such a drop contrasts with the slight variation of T_N using rare earths smaller than Y, and it deserves further investigation.

(14) Shannon, R. D.; *Acta Crystallogr. A* **1976**, *32*, 751.

Conclusions

We have shown that $GdNiO_3$ can be prepared from citrate precursors at moderate O_2 pressures (90 MPa), whereas $DyNiO_3$ must be stabilized under higher hydrostatic pressures in the presence of $KClO_4$. $TbNiO_3$ could not be synthesized. A room-temperature NPD study shows that the Dy perovskite is orthorhombic, as are the previous members of the family, but presents a noticeable distortion of the NiO_6 octahedra, as a consequence of the manifestation of the Jahn−Teller character of Ni^{3+}, giving evidence for the high electron−lattice coupling present in this strongly distorted nickelate. By analogy with previous members of the series, $GdNiO_3$ and $DyNiO_3$ show metal−insulator transitions, above room temperature, characterized by DSC measurements. At lower temperatures ($T_N < T_{MI}$) they exhibit paramagnetic−antiferromagnetic transitions, involving the Ni sublattice, also following the trend established for the lighter members of $RNiO_3$ perovskites. Additionally, susceptibility and specific heat data for $DyNiO_3$ give evidence for the low-temperature long-range magnetic ordering of the Dy^{3+} sublattice.

Acknowledgment. We thank the financial support of CICyT to the project PB97-1181, and we are grateful to ILL for making all facilities available.

CM991033K